

Noise Correlations in a Coulomb Blockaded Quantum Dot

Y. Zhang,¹ L. DiCarlo,¹ D. T. McClure,¹ M. Yamamoto,^{2,3}

S. Tarucha,^{2,4} C. M. Marcus,¹ M. P. Hanson,⁵ and A. C. Gossard⁵

¹*Department of Physics, Harvard University, Cambridge, Massachusetts 02138, USA*

²*Department of Applied Physics, University of Tokyo, Bunkyo-ku, Tokyo 113-8656, Japan*

³*SORST-JST, Kawaguchi-shi, Saitama 331-0012, Japan*

⁴*ICORP-JST, Atsugi-shi, Kanagawa 243-0198, Japan*

⁵*Department of Materials, University of California, Santa Barbara, California, 93106, USA*

(Dated: October 10, 2018)

We report measurements of current noise auto- and cross-correlation in a tunable quantum dot with two or three leads. As the Coulomb blockade is lifted at finite source-drain bias, the auto-correlation evolves from super-Poissonian to sub-Poissonian in the two-lead case, and the cross-correlation evolves from positive to negative in the three-lead case, consistent with transport through multiple levels. Cross-correlations in the three-lead dot are found to be proportional to the noise in excess of the Poissonian value in the limit of weak output tunneling.

Considered individually, Coulomb repulsion and Fermi statistics both tend to smooth electron flow, thereby reducing shot noise below the uncorrelated Poissonian limit [1, 2]. For similar reasons, Fermi statistics without interactions also induces a negative noise cross-correlation in multiterminal devices [1, 2, 3, 4]. It is therefore surprising that under certain conditions, the interplay between Fermi statistics and Coulomb interaction can lead to electron bunching, i.e., super-Poissonian auto-correlation and positive cross-correlation of electronic noise.

The specific conditions under which such positive noise correlations can arise has been the subject of numerous theoretical [5, 6, 7, 8, 9, 10, 11, 12, 13, 14] and experimental [14, 15, 16, 17, 18, 19, 20, 21, 22, 23] studies in the past few years. Super-Poissonian noise observed in MES-FETs [15], tunnel barriers [16] and self-assembled stacked quantum dots [17] has been attributed to interacting localized states [10, 15, 24] occurring naturally in these devices. In more controlled geometries, super-Poissonian noise has been associated with inelastic cotunneling [9] in a nanotube quantum dot [20], and with dynamical channel blockade [11, 12] in GaAs/AlGaAs quantum dots in the weak-tunneling [21] and quantum Hall regimes [22]. Positive noise cross-correlation has been observed in a capacitively-coupled double dot [23] as well as in electronic beam-splitters following either an inelastic voltage probe [5, 6, 7, 8, 19] or a super-Poissonian noise source [18]. The predicted positive noise cross-correlation in a three-lead quantum dot [12] has not been reported experimentally to our knowledge.

This Letter describes measurement of current noise auto- and cross-correlation in a Coulomb-blockaded quantum dot configured to have either two or three leads. As a function of gate voltage and bias, regions of super- and sub-Poissonian noise, as well as positive and negative noise cross-correlation, are identified. Results are in good agreement with a multi-level sequential-tunneling model in which electron bunching arises from dynamical chan-

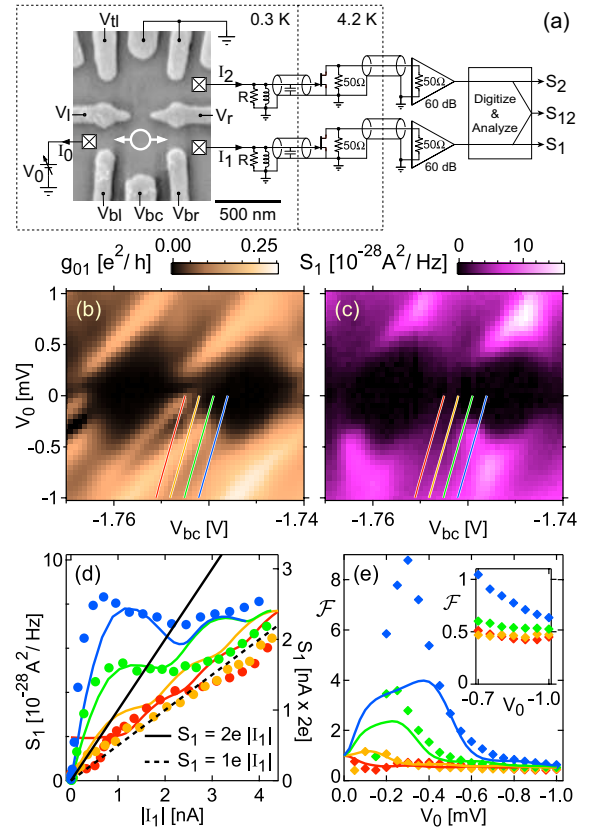


FIG. 1: (a) Micrograph of the device and equivalent circuit near 2 MHz of the noise detection system (see text for equivalent circuit near dc). For the data in Figs. 1 and 2, the V_l - V_r constriction is closed and the dot is connected only to reservoirs 0 and 1. (b, c) Differential conductance g_{01} and current noise spectral density S_1 , respectively, as a function of V_0 and V_{bc} . (d) S_1 versus $|I_1|$ data (circles) and multi-level simulation (solid curves) along the four cuts indicated in (b) and (c) with corresponding colors. Black solid (dashed) line indicates $S_1 = 2e|I_1|$ ($S_1 = 1e|I_1|$). (e) Data (diamonds) and multi-level simulation (solid curves) of the modified Fano factor \mathcal{F} along the same cuts as taken in (d). Inset: detail of \mathcal{F} at high $|V_0|$.

nel blockade [11, 12]. For weak-tunneling output leads, noise cross-correlation in the three-lead configuration is found to be proportional to the deviation of the auto-correlation from the Poissonian value (either positive or negative) similar to the relation found in electronic Hanbury Brown–Twiss (HBT)–type experiments [3, 4, 18].

The quantum dot is defined by gates on the surface of a GaAs/Al_{0.3}Ga_{0.7}As heterostructure [Fig. 1(a)]. The two-dimensional electron gas 100 nm below the surface has density $2 \times 10^{11} \text{ cm}^{-2}$ and mobility $2 \times 10^5 \text{ cm}^2/\text{Vs}$. Leads formed by gate pairs V_l - V_{bl} , V_r - V_{br} , and V_l - V_r connect the dot to three reservoirs labeled 0, 1, and 2, respectively. Plunger gate voltage V_{bc} controls the electron number in the dot, which we estimate to be ~ 100 . The constriction formed by V_{l1} - V_l is closed.

A ³He cryostat is configured to allow simultaneous conductance measurement near dc and noise measurement near 2 MHz [25]. For dc measurements, the three reservoirs are each connected to a voltage amplifier, a current source, and a resistor to ground ($r = 5 \text{ k}\Omega$). The resistor r converts the current I_α out of reservoir α to a voltage signal measured by the voltage amplifier; it also converts the current from the current source to a voltage excitation V_α applied at reservoir α . The nine raw differential conductance matrix elements $\tilde{g}_{\alpha\beta} = dI_\beta/dV_\alpha$ are measured simultaneously with lock-in excitations of $20 \mu\text{V}_{\text{rms}}$ at 44, 20 and 36 Hz on reservoirs 0, 1 and 2, respectively. Subtracting r from the matrix $\tilde{\mathbf{g}}$ yields the intrinsic conductance matrix $\mathbf{g} = [\mathbf{E} + r\tilde{\mathbf{g}}]^{-1} \cdot \tilde{\mathbf{g}}$, where \mathbf{E} is the identity matrix. Ohmic contact resistances ($\sim 10^3 \Omega$) are small compared to dot resistances ($\gtrsim 10^5 \Omega$), and are neglected in the analysis. Values for the currents I_α with bias V_0 applied to reservoir 0 are obtained by numerically integrating $\tilde{g}_{0\alpha}$.

Fluctuations in currents I_1 and I_2 are extracted from voltage fluctuations around 2 MHz across separate resistor-inductor-capacitor (RLC) resonators [Fig. 1(a)]. Power spectral densities $S_{V1,2}$ and cross-spectral density S_{V12} of these voltage fluctuations [25] are averaged over 20 s, except where noted. Following the calibration of amplifier gains and electron temperature T_e using noise thermometry [25], the dot's intrinsic current noise power spectral densities $S_{1,2}$ and cross spectral density S_{12} are extracted by taking into account the feedback [7] and thermal noise from the finite-impedance external circuit [26].

Figure 1(b) shows conductance g_{01} as a function of V_{bc} and V_0 in a two-lead configuration, i.e., with the V_l - V_r constriction closed. The characteristic Coulomb blockade (CB) diamond structure yields a charging energy $E_C = 0.8 \text{ meV}$ and lever-arm for the plunger gate $\eta_{bc} = \Delta\varepsilon_d/(e\Delta V_{bc}) = 0.069$, where ε_d is the dot energy. The diamond tilt $\eta_{bc}/(1/2 - \eta_0)$ gives the lever-arm for reservoir 0: $\eta_0 = \Delta\varepsilon_d/(e\Delta V_0) = 0.3$. As shown in Fig. 1(d), current noise S_1 along selected cuts close to the zero-bias CB peak (red, orange cuts) is below the Pois-

sonian value $2e|I_1|$ at all biases $|I_1|$, while cuts that pass inside the CB diamond (green, blue cuts) exceed $2e|I_1|$ at low currents, then drop below $2e|I_1|$ at high currents. At finite T_e , the current noise $S_1^{\text{P}} = 2eI_1 \coth(eV_0/2k_B T_e)$ of an ideal Poissonian noise source at bias V_0 may exceed $2e|I_1|$ due to the thermal (Johnson) noise contribution [9]. Accordingly, we define a modified Fano factor $\mathcal{F} \equiv S_1/S_1^{\text{P}}$. Figure 1(e) shows regions of super-Poissonian noise, $\mathcal{F} > 1$, when the green and blue cuts are within the CB diamond. For all cuts, \mathcal{F} approaches 1/2 at large bias.

Current noise can also be identified as sub- or super-Poissonian from the excess Poissonian noise $S_1^{\text{EP}} \equiv S_1 - S_1^{\text{P}}$ being negative or positive, respectively. Unlike \mathcal{F} , S_1^{EP} does not have divergent error bars inside the CB diamond, where currents vanish. As shown in Fig. 2(a), in regions where both I_1 and S_1 vanish, S_1^{EP} also vanishes. Far outside the CB diamonds, S_1^{EP} is negative, indicating sub-Poissonian noise. However, S_1^{EP} becomes positive along the diamond edges, indicating super-Poissonian noise in these regions.

We next compare our experimental results to single-level and multi-level sequential-tunneling models of CB transport. The single-level model yields exact expressions for average current and noise [1, 13, 27]: $I_1 = (e/h) \int d\varepsilon \gamma_0 \gamma_1 (f_1 - f_0) / [(\gamma_1 + \gamma_0)^2/4 + (\varepsilon - \varepsilon_d)^2]$, $S_1 = (2e^2/h) \int d\varepsilon \{ \gamma_0^2 \gamma_1^2 \cdot [f_0(1 - f_0) + f_1(1 - f_1)] + \gamma_0 \gamma_1 [(\gamma_1 - \gamma_0)^2/4 + (\varepsilon - \varepsilon_d)^2] \cdot [f_0(1 - f_1) + f_1(1 - f_0)] \} / [(\gamma_1 + \gamma_0)^2/4 + (\varepsilon - \varepsilon_d)^2]^2$, where $\gamma_{0(1)}$ is the tunneling rate to reservoir 0(1) and $f_{0(1)}$ is the Fermi function in reservoir 0(1). The dot energy ε_d is controlled by gate and bias voltages: $\varepsilon_d = -eV_{bc}\eta_{bc} - eV_0\eta_0 - eV_1\eta_1 + \text{const}$. For the multi-level sequential-tunneling model, a master equation is used to calculate current and noise, following Refs. [11, 12, 28]. To model transport, we assume simple filling of orbital levels and consider transitions to and from N -electron states that differ in the occupation of at most n levels above (indexed 1 through n) and m levels below (indexed -1 through $-m$) the highest occupied level in the $(N + 1)$ -electron ground state (level 0) [29].

Super-Poissonian noise in the multi-level model arises from *dynamical channel blockade* [11, 12], illustrated in the diagrams in Fig. 2. Consider, for example, the energy levels and transport processes shown in the green-framed diagram, which corresponds to the location of the green dot on the lower-right edge in Fig. 2(c). Along that edge, the transport involves transitions between the N -electron ground state and $(N + 1)$ -electron ground or excited states. When an electron occupies level 0, it will have a relatively long lifetime, as tunneling out is suppressed by the finite electron occupation in reservoir 1 at that energy. During this time, transport is blocked since the large charging energy prevents more than one non-negative-indexed level from being occupied at a time. This blockade happens dynamically during transport, leading to electron bunching and thus to

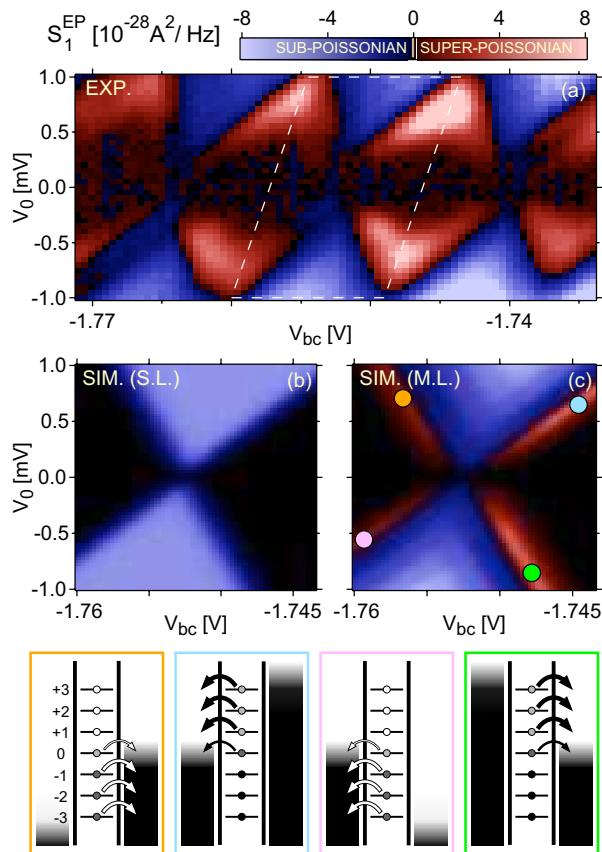


FIG. 2: (a) Excess Poissonian noise S_1^{EP} as a function of V_0 and V_{bc} . Red (blue) regions indicate super(sub)-Poissonian noise. (b, c) Single-level (S.L.) and multi-level (M.L.) simulation of S_1^{EP} , respectively, corresponding to the data region enclosed by the white dashed parallelogram in (a). At the four colored dots superimposed on (c), where S_1^{EP} is most positive, energy diagrams are illustrated in the correspondingly colored frames at the bottom. In these diagrams, black (white) arrows indicate electron (hole) transport; the greyscale color in the reservoirs and inside the circles on each level indicates electron population, the darker the higher.

super-Poissonian noise. At the location of the pink dot on the lower-left edge in Fig. 2(c), the transport involves transitions between the $(N+1)$ -electron ground state and N -electron ground or excited states; a similar dynamical blockade occurs in a complementary hole transport picture. The hole transport through level 0 is slowed down by the finite hole occupation in reservoir 0, modulating the hole transport through negative-indexed levels, thus leading to hole bunching and super-Poissonian noise. Transport at the blue (orange) dot is similar to transport at the green (pink) dot, but with the chemical potentials in reservoirs 0 and 1 swapped. Both experimentally and in the multi-level simulation, S_1^{EP} is stronger along electron edges than along hole edges. This is due to the energy dependence of the tunneling rates: since the positive-indexed electron levels have higher tunneling rates than the negative-index hole levels, the dynamical modulation due to electron transport is stronger for

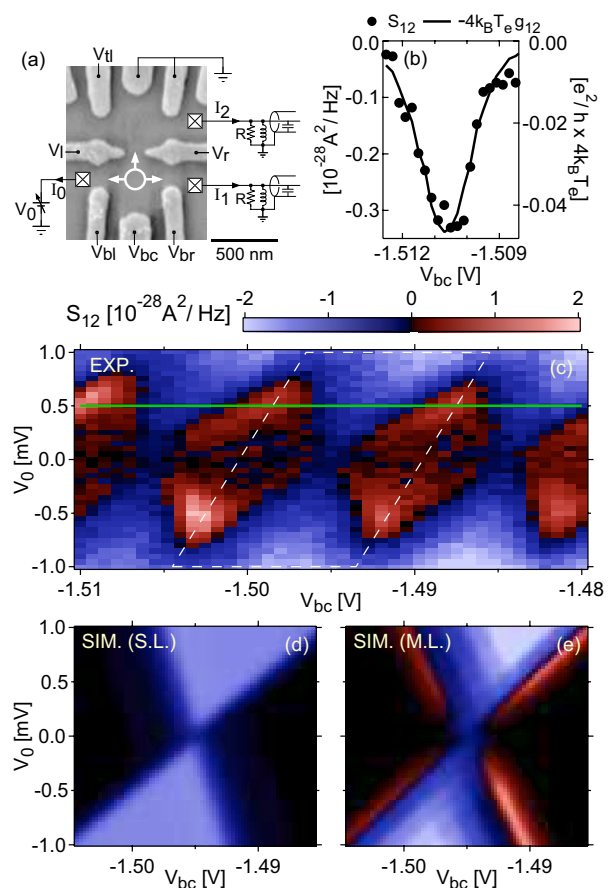


FIG. 3: (a) The device in the three-lead configuration, in which the data for this figure and for Fig. 4 are taken. (b) S_{12} , integrated for 200 s, and $-4k_{\text{B}}T_e g_{12}$ over a CB peak at zero bias. Left and right axes are in different units but both apply to the data. (c) S_{12} as a function of V_0 and V_{bc} . Red (blue) regions indicate positive (negative) cross-correlation. (d, e) Single-level (S.L.) and multi-level (M.L.) simulation of S_{12} , respectively, corresponding to the data region enclosed by the white dashed parallelogram in (c).

electrons than for holes.

We next investigate the three-lead configuration, obtained by opening lead 2 [Fig. 3(a)]. At zero bias, thermal noise cross-correlation is found to be in good agreement with the theoretical value [30], $S_{12} = -4k_{\text{B}}T_e g_{12}$, as seen in Fig. 3(b). To minimize this thermal contribution to S_{12} , output leads are subsequently tuned to weaker tunneling than the input lead ($g_{01} \sim g_{02} \sim 4g_{12}$), for reasons discussed below. Note that as a function of V_{bc} and V_0 , S_{12} [Fig. 3(c)] looks similar to S_1^{EP} [Fig. 2(a)] in the two-lead configuration.

Both the single-level and multi-level models can be extended to include the third lead [12, 27]. Figures 3(d) and 3(e) show the single-level and multi-level simulations of S_{12} , respectively. Similar to the two-lead case, only the multi-level model reproduces the positive cross-correlation along the diamond edges.

To further investigate the relationship between noise

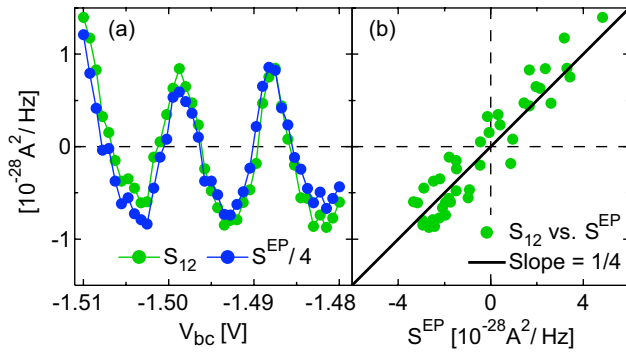


FIG. 4: (a) S_{12} (green) and $S^{\text{EP}}/4$ (blue) as a function of V_{bc} at $V_0 = +0.5$ mV (green horizontal line in Fig. 3(c)). (b) Parametric plot of S_{12} (green circles) versus S^{EP} for the same data as in (a). The solid black line has a slope of $1/4$, the value expected for a 50/50 beam-splitter.

auto- and cross-correlation, we compare S_{12} to the total excess Poissonian noise, $S^{\text{EP}} \equiv S_1 + S_2 + 2S_{12} - 2e(I_1 + I_2) \coth(eV_0/2k_B T_e)$, measured in the same three-lead configuration. Figure 4 shows S^{EP} and S_{12} , measured at fixed bias $V_0 = +0.5$ mV. The observed proportionality $S_{12} \sim S^{\text{EP}}/4$ is reminiscent of electronic HBT-type experiments [3, 4, 18], where noise cross-correlation following a beam-splitter was found to be proportional to the total output current noise in excess of the Poissonian value, with a ratio of $1/4$ for a 50/50 beam-splitter. In simulation, we find that this HBT-like relationship holds in the limit $g_{01} \sim g_{02} \gg g_{12}$ (recall that $g_{01} \sim g_{02} \sim 4g_{12}$ in the experiment); on the other hand, when $g_{01} \sim g_{02} \sim g_{12}$, thermal noise gives a negative contribution that lowers S_{12} below $S^{\text{EP}}/4$, as we have also observed experimentally (not shown). The implications are that first, with weak tunneling output leads, the three-lead dot behaves as a two-lead dot followed by an ideal beam-splitter, and second, the dynamical channel blockade that leads to super-Poissonian noise in the two-lead dot also gives rise to positive cross-correlation in the three-lead dot.

We thank N. J. Craig for device fabrication and H.-A. Engel for valuable discussions. We acknowledge support from the NSF through the Harvard NSEC, PHYS 01-17795, DMR-05-41988, DMR-0501796. M. Yamamoto and S. Tarucha acknowledge support from the DARPA QuIST program, the Grant-in-Aid for Scientific Research A (No. 40302799), the MEXT IT Program and the Murata Science Foundation.

[1] Ya. M. Blanter and M. Büttiker, Phys. Rep. **336**, 1 (2000). Ya. M. Blanter, cond-mat/0511478 (2005).

- [2] M. Büttiker, Phys. Rev. Lett. **65**, 2901 (1990); M. Büttiker, Phys. Rev. B **46**, 12485 (1992).
- [3] M. Henny *et al.*, Science **284**, 296 (1999). S. Oberholzer *et al.*, Physica E **6**, 314 (2000).
- [4] W. D. Oliver *et al.*, Science **284**, 299 (1999).
- [5] C. Texier and M. Büttiker, Phys. Rev. B **62**, 7454 (2000).
- [6] M. Büttiker, in *Quantum Noise in Mesoscopic Physics*, NATO Science Series II **97**, edited by Yu. V. Nazarov (Kluwer, Dordrecht, 2003), cond-mat/0209031.
- [7] S.-T. Wu and S. Yip, Phys. Rev. B **72**, 153101 (2005).
- [8] V. Rychkov and M. Büttiker, Phys. Rev. Lett. **96**, 166806 (2006).
- [9] E. V. Sukhorukov *et al.*, Phys. Rev. B **63**, 125315 (2001).
- [10] G. Kiesslich *et al.*, Phys. Rev. B **68**, 125320 (2003).
- [11] W. Belzig, Phys. Rev. B **71**, R161301 (2005).
- [12] A. Cottet *et al.*, Phys. Rev. B **70**, 115315 (2004). A. Cottet *et al.*, Phys. Rev. Lett. **92**, 206801 (2004).
- [13] A. Thielmann *et al.*, Phys. Rev. Lett. **95**, 146806 (2005).
- [14] G. Iannaccone *et al.*, Phys. Rev. Lett. **80**, 1054 (1998).
- [15] S. S. Safonov *et al.*, Phys. Rev. Lett. **91**, 136801 (2003).
- [16] Y. Chen and R. A. Webb, Phys. Rev. B **73**, 35424 (2006).
- [17] P. Barthold *et al.*, Phys. Rev. Lett. **96**, 246804 (2006).
- [18] Y. Chen and R. A. Webb, Phys. Rev. Lett. **97**, 66604 (2006).
- [19] S. Oberholzer *et al.*, Phys. Rev. Lett. **96**, 46804 (2006).
- [20] E. Onac *et al.*, Phys. Rev. Lett. **96**, 26803 (2006).
- [21] S. Gustavsson *et al.*, Phys. Rev. B **74**, 195305 (2006).
- [22] O. Zarchin *et al.*, Phys. Rev. Lett. **98**, 66801 (2007).
- [23] D. T. McClure *et al.*, Phys. Rev. Lett. **98**, 56801 (2007).
- [24] M. Eto *et al.*, Jpn. J. Appl. Phys. **36**, 4004 (1997).
- [25] L. DiCarlo *et al.*, Rev. Sci. Inst. **77**, 73906 (2006).
- [26] The dot's intrinsic current noises are extracted by solving the Langevin equations for finite-impedance external circuits [1]:

$$\begin{aligned} S_1 &= a_{11}^2 S_{V1} + a_{21}^2 S_{V2} + 2a_{11}a_{21} S_{V12} - 4k_B T_e / R \\ S_2 &= a_{12}^2 S_{V1} + a_{22}^2 S_{V2} + 2a_{12}a_{22} S_{V12} - 4k_B T_e / R \\ S_{12} &= a_{11}a_{12} S_{V1} + a_{21}a_{22} S_{V2} + (a_{11}a_{22} + a_{12}a_{21}) S_{V12}, \end{aligned}$$

where $a_{11(22)} = 1/R - g_{11(22)}$, $a_{12(21)} = -g_{12(21)}$ and R is the RLC resonator parallel resistance.

- [27] H.-A. Engel, Ph.D. thesis, University of Basel (2003).
- [28] S. Hershfield *et al.*, Phys. Rev. B **47**, 1967 (1993).
- [29] For computational reasons, we limit the calculation to $n = m = 3$. For simplicity, we assume equal level spacings, symmetric tunnel barriers, and an exponential dependence of the tunneling rates on level energy: $\Delta \varepsilon^l \equiv \varepsilon_d^l - \varepsilon_d^0 = l \times \delta$ and $\gamma_0^l = \gamma_1^l = \Gamma \exp(\kappa \Delta \varepsilon^l)$, where $l = -3, \dots, 0, \dots, 3$ is the level index, ε_d^l is the energy of level l , and $\gamma_{0(1)}^l$ is the tunneling rate from level l to reservoir 0(1). We chose $\delta = 150 \mu\text{eV}$, $\Gamma = 15 \text{ GHz}$ and $\kappa = 0.001 (\mu\text{eV})^{-1}$ to fit the data in Figs. 1(d) and 1(e).
- [30] At zero bias, the fluctuation-dissipation theorem requires $S_{12} = -2k_B T_e (g_{12} + g_{21})$, but $g_{12} = g_{21}$ at zero bias and zero magnetic field. However, the fact that $g_{12} \neq g_{21}$ at finite bias, observed experimentally, requires knowledge of the full conductance matrix to properly extract $S_{1,2}$ and S_{12} [26].